INTERNATIONAL JOURNAL OF AUTOMOTIVE AND MECHANICAL ENGINEERING
ISSN: 2229-8649 e-ISSN: 2180-1606
VOL. 21, ISSUE 3, 2024, 11469 – 11485
DOI: https://doi.org/10.15282/ijame.21.3.2024.2.0885

RESEARCH ARTICLE

Experimental Evaluation of Damping and Stiffness in Optimized Active Sport Utility Vehicle Suspension Systems

Shaimaa Awad[1]*, Eid Ouda Awad[1], Wael Galal Ata[2], Samir M. El-Demerdash[1], Ahmed Shehata Gad[1]

[1]Faculty of Engineering at Mataria, Helwan University, Cairo, Egypt
[2]Head of Tanks Department, Mechanical Engineering Branch, Military Technical College, Cairo, Egypt

ABSTRACT - On a flat city road, the specificity of the suspension poses a challenge. Sport utility vehicles (SUVs) have less flexibility compared to regular cars, despite providing a firm grip on asphalt and concrete. Constant adjustments to the center of gravity of SUVs are necessary. Surprisingly, they are less reliable and stable in urban settings due to this characteristic. In this study, a mathematical model of the suspension system of SUVs based on the Newtonian approach is introduced and validated with data from experiments carried out by the MTS machine system on the mono-tube (oil/air) mixed damper element. The model accurately predicts the performance of this damper, commonly used in SUVs, across various operating conditions, including different frequencies. A coil spring element, serving as a passive suspension unit with this damper, is also tested experimentally under similar conditions. By integrating passive suspension elements with the active actuator, the proposed modified design reduces the power consumption needed for the actuator to function and ensures a certain level of reliability. The effectiveness and performance of the modified active suspension system in comparison to the traditional passive suspension system are assessed using three different strategies: hybrid PID-LQR, linear quadratic regulator (LQR), and proportional-integral-derivative (PID). The genetic algorithm is utilized to determine the optimal parameter values for each controller by minimizing a cost function, maximizing performance, and minimizing energy consumption. Simulation results demonstrate that the active suspension system controlled by the PID-LQR controller offers significantly improved ride comfort and vehicle stability compared to other systems. This suggests that the performance of the active suspension system is greatly enhanced by the combined application of the hybrid PID-LQR controller compared to other systems.

ARTICLE HISTORY
Received : 09th Mar. 2024
Revised : 06th June 2024
Accepted : 11th June 2024
Published : 20th Sept. 2024

KEYWORDS
SUV coil spring
SUV oil/air mixed damper
Vehicle suspension model
Hybrid controller design

1. INTRODUCTION

Hydraulic shock absorbers are used to reduce impact and vibrations to create smoother motion under various circumstances. They also help to maintain the stability and control of the vehicle by minimizing the effects of bumps and uneven road surfaces [1-3]. There are three primary approaches that have been the focus of recent published work on the behavior of automotive shock absorbers for passenger cars, each with varying degrees of complexity: (1) shock absorbers are physically tested as part of experimental studies under various circumstances, including shifting loads, speeds, and road surfaces [4-5]. (2) The creation of analytical models to simulate the behavior of automotive shock absorbers is another strategy [1]. Through analytical modeling, shock absorbers' dynamic responses to various inputs and operating conditions can be examined, allowing for a theoretical understanding of their behavior [2]. (3) The behavior of automobile shock absorbers has been simulated by numerical techniques. Various techniques are employed to simulate the intricate behavior of shock absorbers, including computational fluid dynamics (CFD), finite element analysis (FEA), and multibody dynamics simulation [3]. Without any parameter adjustment, accurate agreement is obtained between the model results and test data for damper velocities up to ±1 m/s for a wide range of input parameters, such as valve combination, stroke conditions, gas charge pressure, and damper size [9]. A moderate deviation arises for certain valve combinations when the stroke speed exceeds ±1 m/s because of the model's simplifications. Another significant factor that impacts the predicted performance of an oil/air mixed damper is cavitation [10]. The emergence and disintegration of bubbles during cavitation can cause uncertainty and make it difficult to forecast the performance of dampers with precision. The kind of damper, the operating environment, and the degree of cavitation all affect how dampers behave when subjected to cavitation. Bubble formation has the potential to impair the damper's overall performance, stability, and efficiency by obstructing the airflow through it. Along with shock absorbers, coil springs play a crucial role in suspension systems by supporting the car's weight and providing a cushioning effect to absorb impacts from the road [4]. The dynamic properties of a coil spring, including its stiffness, can vary depending on the exciting frequency [5]. The stiffness of a coil spring is influenced by several factors, including the mass distribution of the spring and the frequency at which it is excited [6]. The stiffness of a coil spring is typically characterized by its spring rate, which represents the amount of force required to compress or extend the spring by a certain distance [7].

***CORRESPONDING AUTHOR | S. Awad** | ✉ ahmed01140938289@gmail.com

However, at different frequencies of excitation, the behavior of the spring can change due to dynamic effects [8]. At lower frequencies, the mass distribution and inertia of the spring may have a more significant impact on its stiffness. As the excitation frequency increases, the dynamic response of the spring, including its natural frequency and resonance behavior, becomes more pronounced. This phenomenon is known as dynamic stiffness variation, where the effective stiffness of the spring changes with the frequency of excitation. At certain frequencies, the spring may exhibit different stiffness characteristics, including softening or hardening effects, due to dynamic interactions between the mass distribution, inertia, and the applied forces. When a vehicle encounters random track irregularities, the excitation forces can lead to the excitation of specific structural modes of the coil spring at frequencies. This phenomenon can have significant effects on the stiffness and fatigue life of the spring [9].

It's important to note that advancements in suspension technology have led to the development of active and semi-active suspension systems, which incorporate electronic control systems to dynamically adjust the suspension characteristics. To meet the increased energy requirements of active suspensions, a high-power supply is also necessary [10]. Active suspensions are now unaffordable for vehicle applications due to the additional cost of this power supply in the implementation process [11]. However, passive suspension systems continue to be widely used due to their simplicity, durability, and effectiveness in meeting the demands of everyday driving [12]. Additionally, a suspension design that is more optimized and balanced is made possible by the combination of passive and active components [13]. Two important goals are achieved by combining passive suspension components with active components: increasing reliability and lowering power consumption. The system's performance can be further enhanced through the design and implementation of active elements, which are made possible by the passive elements' baseline level of safety and performance. The system can function at its best while maintaining efficiency and safety thanks to this integration [14]. Ride comfort is a crucial component that directly affects how content car owners are. Less fatigue and a more pleasurable trip are guaranteed by a comfortable and smooth ride. However, attaining the ideal level of comfort during a ride can frequently result in a vehicle losing stability, which is essential for safe handling and maneuverability [15]. On the other hand, maintaining vehicle stability is crucial to guaranteeing the safety of both drivers and passengers. It entails keeping control of the car under different driving circumstances, like braking, acceleration, and corners. A stable car improves handling, lowers the chance of collisions, and increases general road safety [16].

The trade-off between competing requirements in active vehicle suspension systems has been addressed by the introduction of several control techniques [17]. By skillfully striking a balance between ride comfort, handling, and vehicle stability, these methods seek to improve the performance of the suspension system. Adaptive control techniques refer to the capacity of such systems to continuously modify their parameters in response to feedback received in real-time from sensors [18]. By continuously adjusting, the suspension system can adjust to changing driving dynamics, vehicle speed, and road conditions, ultimately resulting in the best possible balance between comfort and performance [19]. One of the key advantages of adaptive control is its ability to enhance the overall ride quality. By constantly monitoring and analyzing road conditions, the suspension system can automatically adjust its parameters to absorb bumps and vibrations, resulting in a smoother ride for the occupants [20]. This is particularly beneficial when driving on uneven or rough surfaces, where the suspension can quickly react to changes in the road profile, ensuring a more comfortable experience. Moreover, adaptive control also plays a crucial role in improving vehicle handling and stability [21]. By continuously receiving feedback from various sensors, such as wheel speed sensors and accelerometers, the suspension system can adapt its parameters to provide optimal traction and stability during cornering, braking, or acceleration. This enables the vehicle to maintain better control and responsiveness, enhancing both safety and performance. Another important aspect of adaptive control is its ability to optimize the suspension system's behavior based on the driver's preferences and driving style [22]. By analyzing inputs from sensors and monitoring driver actions, such as steering and braking, the system can automatically adjust the suspension parameters to match the driver's desired level of comfort and performance. This personalized approach ensures that the suspension system adapts to the driver's needs, providing a more engaging and satisfying driving experience [23].

The automobile industry market is geared toward SUVs. The size, versatility, sturdy feel, and impressive view that characterize this class of cars appeal to customers [24]. Specifically, a higher propensity to roll over than is typical for an automobile has resulted from the combination of a large weight and a relatively high center of gravity in these vehicles [25]. Suspension designers have been pushed to consider alternatives to traditional suspension systems in order to preserve the high safety standards of automobiles while maintaining the level of comfort that consumers expect from cars in this class [26]. SUVs with active suspension control have an active actuator that can produce the best control forces based on input parameters, enhancing the vehicle's handling stability and comfort while being driven [27]. In order to satisfy the various comfort and safety needs of active suspension under various road conditions performance criteria, a fuzzy proportional-integral differential (PID) control approach based on road surface estimate is used [28]. By considering actuator saturation, suspension non-linearity, fuzzy sliding mode control, and self-immunity control, the active immunity controller is made to increase driver comfort [29]. In order to effectively reduce the effects of uncertainty and nonlinear conditions on suspension control performance, fuzzy rules are integrated with the fractional order PD control approach to regulate active suspension [30]. To increase the stability of suspension control, nonlinear suspension control was converted into a convex optimization problem with linear matrix inequality constraints. A multivariate predictive control technique was then created for nonlinear suspensions. For an uncertain active vehicle suspension system, finite frequency fuzzy H∞ control efficiently optimizes the parametrization from external disturbance to regulated output within the

comfort frequency to enhance suspension smoothness [31]. Additionally, road surface and system state variables are employed as inputs to change the active suspension control modes in response to varying road conditions in order to increase comfort [32]. Despite the fact that fuzzy controllers are robust, have low overshoot, and can overcome non-linearity in the system, more quantization steps are still needed to improve fuzzy control accuracy by expanding the rule search range, slowing down decision-making, and managing control in highly motorized vehicles [33]. The design of fuzzy PID control techniques for active car suspensions has garnered a lot of attention because they can handle the conflicts between control accuracy and speed and mitigate the effects of control parameter uncertainty [34]. The fuzzy PID controller uses fuzzy inference choices from system failures and changes in external excitation to automatically modify the PID parameters online to fit the operating environment and the changing system parameters. While the previously mentioned techniques significantly enhance the precision and flexibility of suspension control, they are limited to mitigating uncertainty within their own parameters. They are not capable of responding promptly to changes in external excitations without actively modifying control parameters beforehand.

In this study, the suspension system used for SUVs is replaced with an active suspension system managed by an improved PID-LQR controller, offering a novel method for improving vehicle stability and ride comfort. By utilizing the Genetic Algorithm (GA), the controller settings are optimized to minimize the goal function. To further illustrate the efficacy of the proposed system, the study evaluates the performance of the active suspension in SUVs with optimal PID, LQR, and PID-LQR alternative controllers against that of the passive suspension system. Through experimental testing, it was discovered that the oil/air mixed damper and coil spring elements commonly found in SUVs have baseline values for the quarter-car model characteristics. The SUV suspension can be significantly enhanced by incorporating the dynamics of the active actuator, which effectively balances the passive components. In recent decades, an evolution has unfolded within the manufacturing sector, transitioning from traditional mass production methodologies towards bespoke manufacturing approaches and evolving from centralized production frameworks to distributed, cloud-based manufacturing ecosystems [1]. This transformation has been catalyzed by the advent of Service-Oriented Cloud Manufacturing (CMfg), a model that epitomizes the convergence of flexibility, resource sharing, and the delivery of manufacturing capabilities as services via the industrial internet [2]. Simultaneously, the emergence of 4D printing [3] technology, which extends beyond the capabilities of 3D printing by integrating the temporal dimension into the fabrication process, represents a significant advancement. This innovation enables materials to be designed with the inherent capacity to alter their configuration, properties, or functionality upon exposure to predetermined stimuli over time, thus facilitating the creation of objects equipped to adapt, self-organize, or transmute in response to external environmental variables.

The amalgamation of cloud manufacturing with 4D printing technologies marks a pivotal convergence within the realm of contemporary manufacturing, blending the digital with the tangible to foster the development of intelligent, versatile, and intricate products. This fusion harbors the potential to revolutionize our perceptions concerning product lifecycle management, supply chain dynamics, and the foundational principles of product design and functionality. This paper endeavors to scrutinize service portfolio optimization [4] within the domain of cloud manufacturing, with a particular focus on services allied to 4D printing. It presents a modeling approach that coordinates and optimizes the service composition of cloud-based 4D printing, achieving multiobjective optimization. It postulates that leveraging a multiobjective methodology facilitated by the Non-dominated Sorting Genetic Algorithm III (NSGA III) [5] could markedly augment the optimization of service portfolios associated with 4D printing. The objective transcends mere cost and quality considerations to include an assessment of the portfolio's adaptability and resilience in the face of demand volatility and resource availability fluctuations, thereby addressing the limitations inherent in extant procedural models.

2. SUVs COIL SPRING

When using an oil/air mixed damper as the suspension unit, one crucial component that must be carefully evaluated is the coil spring based on dynamic stiffness. As illustrated in Figure 1, the MTS 852 machine system also conducts numerous tests as part of this evaluation. The tests performed on the coil spring involve subjecting it to varying loads and measuring the corresponding displacements. The operating length is utilized to determine the actual performance of the coil spring, specifically based on the suspension working space in the SUVs case study. This spring is affixed to the MTS 852 machine system by the upper and lower fixed mounts. The upper fixed mount is responsible for securely holding the upper section of the spring in place. It serves as a stable anchor point, preventing any undesired movement or dislodgement. The upper fixed mount is strategically positioned to offer maximum stability to the spring, ensuring the optimal performance of the MTS 852 machine system. The lower fixed mount complements the upper fixed mount by securing the lower section of the spring. It is designed to firmly keep the spring in position, preventing any unnecessary vibrations or shifts.

By analyzing the data presented from the MTS 852 machine system, we can better understand the performance characteristics and dynamic properties of the coil springs used in SUVs. Figure 2 shows a linear fit of the experimental force-displacement plot. This indicates a direct relationship between the force exerted and the resulting displacement. The plot displayed a straight line, suggesting that as the applied force increased, the displacement also increased proportionally. Such a linear relationship is commonly observed in systems where the applied force is directly proportional to the resulting displacement. Analyzing the slope of the line provides valuable information about the stiffness or compliance of the system. The linear fit conducted on the force-displacement plot enables a quantitative

understanding of the relationship between these variables and serves as a foundation for further analysis and interpretation of the experimental results.

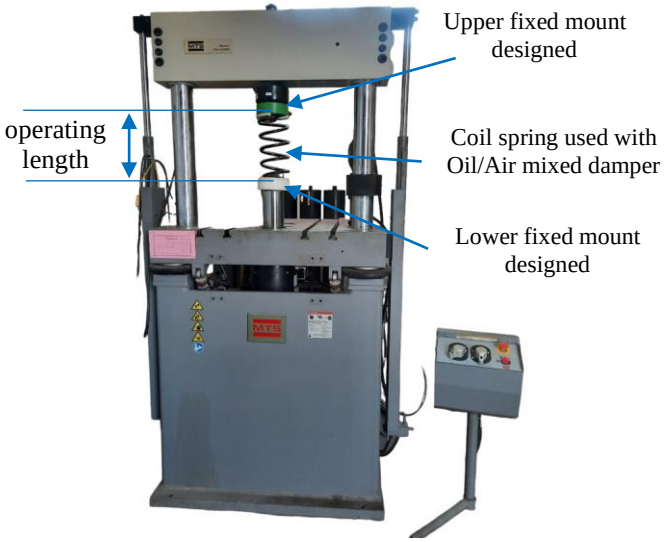

Figure 1. Experimental set-up used to evaluate the dynamic stiffness of a coil spring

From the analysis of the (a) and (c) graphs presented in Figure 2, it is evident that the force-displacement loop at a frequency of 1Hz, with an amplitude of 24 mm, displayed a velocity of approximately 70 mm/sec. This observation indicates the relationship between force and displacement under these specific conditions. At the initial moment of 0 seconds, the exciter in the MTS 852 machine system is initiated with an operating length of 2.9. This value represents the force exerted by the exciter on the system. As time progresses, the operating length gradually decreases. By the time 1 second has elapsed, the force exerted by the exciter reduces to a value slightly lower than the initial 2.9. The exact value at this point is not specified, but it is within the range of 2.9 to 2.45. As the second-second mark is reached, the operating length of the exciter in the MTS 852 machine system decreases further. At this point, the force exerted by the exciter is precisely 2.45. This value represents the final operating length within the specified time frame of 3 seconds.

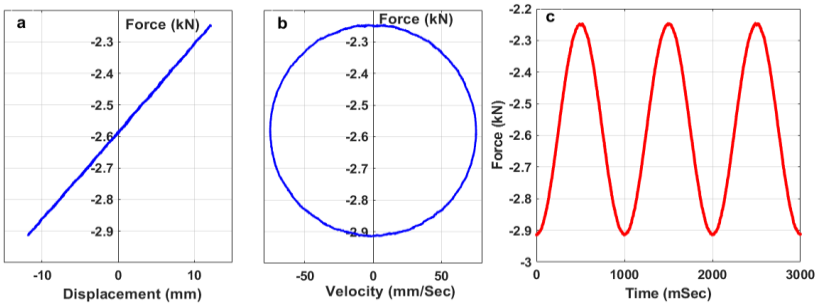

Figure 2. Performance of the proposed coil spring at 1 Hz: (a) force–displacement; (b) force–velocity; (c) force–time

If the spring withstands the applied forces within the specified range without any signs of failure or exceeding the acceptable limits, it can be deemed suitable for SUVs. However, if any issues or deviations are identified, further adjustments or modifications may be required to meet the required performance criteria. From the analysis of the (a) and (c) graphs in Figure 3, it is evident that the force-displacement loop at a frequency of 2 Hz, with an amplitude of 24 mm, displayed a velocity of approximately 150 mm/sec. It is essential to conduct rigorous testing on the coil springs to obtain an accurate evaluation of spring phenomena. The proposed spring will be tested within a range of 2.35 to 2.9. This range has been determined based on the operating range suitable for SUVs.

In Figure 4(a)-(c), an interesting observation can be made regarding the impact of different frequencies on the velocity and force of a certain phenomenon. Specifically, at frequencies of 3 Hz, 6 Hz, 8 Hz, and 11 Hz, it is worth noting that the phenomenon exhibits the ability to generate higher velocity while maintaining the same range of force as compared to frequencies of 1 Hz and 2 Hz. The rate of force generated by SUVs springs refers to the amount of force required to compress or extend the spring based on different amplitudes. This rate is determined by various factors, including the design of the spring, the material used, and the overall suspension setup of the vehicle. SUV springs are made to help cushion passengers from road imperfections and bumps. Manufacturers carefully tune the rate of force generated by SUV springs to find the optimal balance between comfort and control. This involves considering factors such as the weight distribution of the vehicle, the intended use, and the desired ride characteristics. This helps to minimize the impact felt by the driver and passengers, resulting in a smoother and more comfortable ride.

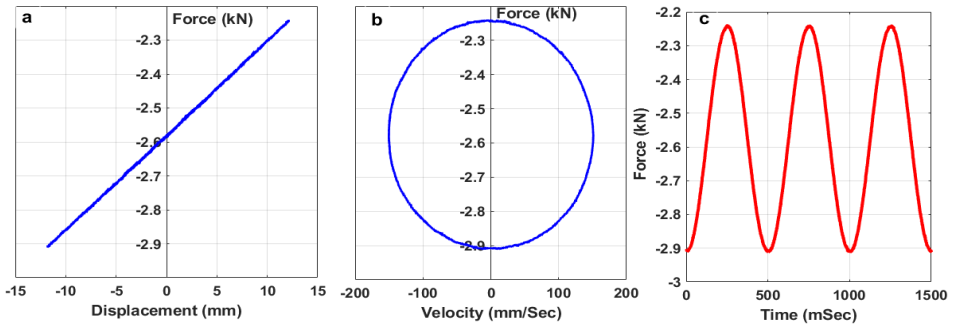

Figure 3. Performance of the proposed coil spring under 2 Hz: (a) force-displacement; (b) force-velocity; (c) force-time

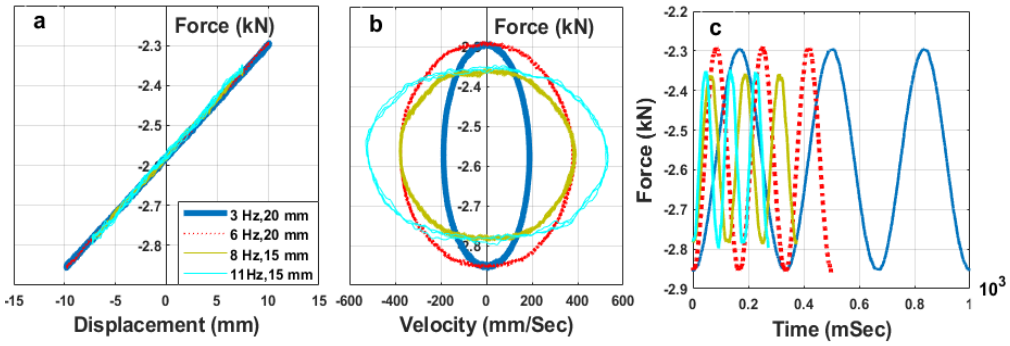

Figure 4. Performance of proposed coil spring under 3 Hz, 6 Hz, 8 Hz, and 11 Hz: (a) force–displacement; (b) force–velocity ;(c) force–time

Figure 5(a)-(c) displays the characteristic curves of the coil spring during the transient case. In this case, the frequency ranges from 0 sec to 6 sec, with a constant value of 1 Hz and an amplitude of 24 mm. From 6 sec to 13 sec, the frequencies vary between 2 Hz and 3 Hz, with an amplitude of 20 mm. Finally, from 13 sec to 16 sec, the frequency is set at 8 Hz, while the amplitude decreases to 15 mm. Figure 5(a) shows that the force-displacement loop remains linear within a range of -11 mm to 11 mm. The graph clearly illustrates the relationship between force and displacement, indicating that as the displacement increases, so does the force exerted. This linear relationship holds true throughout the specified range of displacement, suggesting a consistent behavior of the system. The graph provides valuable insights into the system's response to varying displacements, allowing for a better understanding of its mechanical properties. Figure 5(b) provides valuable insights into the relationship between force and velocity. As the force increases, the velocity follows suit and shows a corresponding increase. This direct relationship can be observed by the linear progression of the data points on the graph. The steeper the slope of the line, the greater the increase in velocity with each increment in amplitude.

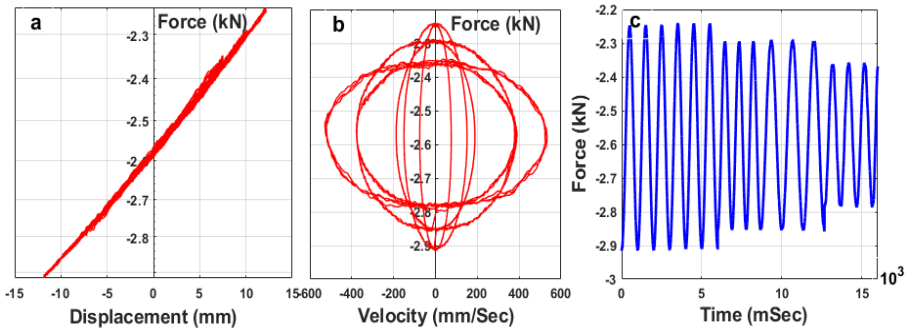

Figure 5. Performance of coil spring with a composed signal of 1 Hz (24 mm), 2 Hz (20 mm), 3 Hz (20 mm), 8 Hz (20 mm), and 8 Hz (15 mm) generated: (a) displacement of force, (b) velocity of force, and (c) displacement of the MTS 852 actuator's applied force

3. SUVs OIL/AIR MIXED DAMPER

3.1 Configuration of Oil/Air Mixed Damper

The oil/air mixed damper's performance is evaluated using the MTS 852 damper test system, as shown in Figure 6. The two main components of this apparatus are the loading unit and the hydraulic power supply unit. The loading unit comprises the load frame, crosshead lift and lock, force transducer, actuator, three-stage servo valve, hydraulic manifold, and accumulators, making it the primary element of the system. A fixed-volume pump is utilized in the hydraulic power supply (HPS) model to provide fluid flow rates of 38 liters per minute and 80 liters per minute, respectively. The output

fluid, which is filtered to a size of 3 microns, is controlled by servo valves to precisely meet the system's requirements. The motor starter box settings enable the HPS to operate at either high or low pressure. The output high-pressure mode is regulated to a maximum suggested pressure of 21 MPa, while the output low-pressure mode is typically set to one MPa. A pressure gauge indicates the output pressure and a secondary pilot valve maintains the operating pressure below a set limit.

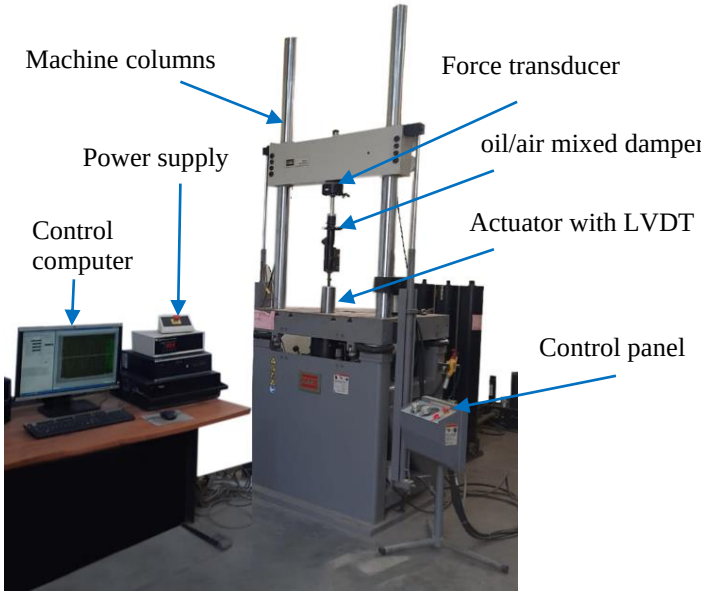

Figure 6. The MTS device used to test the oil/air mixed damper in various scenarios

3.2 Formulation of an Oil/Air Mixed Damper Model

The damping force generated by the oil/air mixed damper model can be calculated using the following nonlinear mathematical equations:

$$F_d = P_1(A_P - A_r) - P_2A_p - sign\left(\frac{dx_1}{dt}\right)F_{f1} - sign\left(\frac{dx_2}{dt}\right)F_{f2} + P_{03}A_r \tag{1}$$

$$x_1 = A(1 - \sin(2\pi ft) \tag{2}$$

$$\frac{dx_2}{dt} = -\frac{1}{A_p} \times \frac{dV_3}{dt} \tag{3}$$

$$\frac{dV_3}{dt} = -\frac{1}{n} \times V_{o3} \times P_{o3}^{\frac{1}{n}} \times P_3^{-\left(\left(\frac{1}{n}\right)+1\right)} \times \frac{dP_3}{dt} \tag{4}$$

Given the adiabatic process assumption, the gas volume may be expressed as

$$P_{03}V_{03}^n = P_3V_3^n \tag{5}$$

where the damping force is F_d, F_{f1} and F_{f2} are the friction forces generated by sliding motions, A_P is the cross-sectional area of the pressure tube, A_r is the cross-sectional area of the piston rod, x_1 is the sinusoidal stroke in time, x_2 is the displacement of the floating piston, P_1 is the pressure in the extension chamber, P_2 is the pressure in the compression chamber, P_{03} is the initial gas (air) pressure, and V_{o3} is the initial volume of the air chamber. P_3 and V_3 are the pressure and volume of gas under both extension and compression.

For the floating piston, the equation of motion is as follows:

$$(P_2 - P_3)\,A_P - sign(\frac{dx_2}{dt})F_{f2} = m_2\frac{d^2x_2}{dt^2} \tag{6}$$

The continuity equations for extension and compression chambers can be stated under isothermal circumstances.

$$Q_1 = \left(A_p - A_r\right)\frac{dX_1}{dt} + \frac{1}{\beta}((A_p - A_r)X_1 + V_{o1})\frac{dP_1}{dt} \tag{7}$$

$$Q_2 = A_p(\frac{dX_2}{dt} - \frac{dX_1}{dt}) + \frac{1}{\beta}((V_{02} - A_pX_1 + V_{03} - V_3)\frac{dP_2}{dt} \tag{8}$$

The overall volumetric flow rate can be defined by the following across the orifices:

$$Q_i = Q_1 + Q_2 \tag{9}$$

Both the fixed and variable orifices use the usual orifice formulae for turbulent flow.

$$Q_i(P_1, P_2) = C_{di} A_i sign(P_2 - P_1) \sqrt{\frac{2}{\rho_{oil}} |P_2 - P_1|} \tag{10}$$

The pressure force is also formulated by

$$F_p = A_{in} |P_2 - P_1| \tag{11}$$

The momentum force is given as

$$F_m = \frac{\rho_{oil} Q_2^2}{A_{in}} \tag{12}$$

the ratio between momentum force and pressure force is described as

$$\frac{F_m}{F_p} = 2C_{d2}^2 \left(\frac{A_2}{A_{in}}\right)^2 \tag{13}$$

$$A_2 = 2\pi a(\omega_{max} - \omega_o) \tag{14}$$

where: Q_1 is the rate of volumetric flow within the extension chamber, Q_2 represents the compression chamber's volumetric flow rate, β represents the oil's bulk modulus, C_{di} is the discharge coefficient, A_i is the orifice area, ρ_{oil} is the density of the oil, A_{in} is the effective pressure area on the disk, A_2 is the orifice area created by the disk deflection, ω_{max} is the maximum deflection of the disk in the fully closed position, ω_o is the disk's initial deflection when it is fully closed, and a represents the disk valve's outer radius.

Table 1. Oil/air mixed damper parameters used in numerical simulation

Symbol	Description	Value	Unit
F_{f1}	Force of friction between the cylinder and piston rod	10	N
F_{f2}	Force of friction between the cylinder and floating piston rod	1	N
A_P	Pressure tube's cross-sectional area	16	cm^2
A_r	Area of the piston rod's cross-section	12.8	cm^2
P_{03}	The initial gas (air) pressure	350	psi
V_{o1}	Initial volume of extension chamber	160	cm^3
V_{02}	Initial volume of compression chamber	130	cm^3
V_{03}	Initial volume of air chamber	70	cm^3
n	Index of Adiabatic	1.4	-
β	Bulk modulus of a fluid at atmospheric pressure	1.5×10^9	Pa
ρ_{oil}	Density of oil under atmospheric pressure	890	kg/m^3

3.3 The Oil/Air Mixed Damper's Validation Model

Figure 7(a)-(h) displays the force-displacement curves for the mathematical model in comparison with the test results. The mathematical model successfully replicated the test results across various displacement values, with the curves closely resembling the recorded sets of results. The mathematical model consistently recreated the force-displacement curves of the test results, affirming its validity. However, the test results indicated a decrease in the force-displacement curve at specific displacement values. The loops observed in the curves are a result of the different frequencies and a constant amplitude (10 mm). These loops are documented to assess the accuracy and precision of the collected data. Each loop corresponds to the use of different frequencies to measure the curve's amplitude. The amplitude of the curves remains steady at 10 mm throughout the process, serving as a reference point for comparison. The loops are documented and analyzed to evaluate data accuracy, enabling a more precise interpretation of the data and the identification of any potential issues. This analysis allows for the accurate measurement of amplitude at various frequencies.

Graph (a) illustrates the performance of the oil/air mixed damper at a frequency of 0.05 Hz compared to the mathematical model. The performance shows rapid recycling and suggests that the mathematical model is at the same level. Graph (b) displays the performance of the oil/air mixed damper at 0.5 Hz. The performance slightly increases from graph (a) and indicates that the mathematical model is starting to respond more effectively. Graph (c) demonstrates the performance of the oil/air mixed damper at 2 Hz. It shows a slight performance increase compared to the previous graph, implying that the mathematical model is not as effective in responding to this frequency. Graph (d) exhibits the

performance of the oil/air mixed damper at 4 Hz. The performance significantly increases from graph (c), suggesting that the mathematical model is responding well to this frequency. Graph (e) depicts the performance of the oil/air mixed damper at 6 Hz. The performance slightly increases from graph (d) and indicates that the mathematical model is further responding to this frequency. Graph (f) showcases the performance of the oil/air mixed damper at 8 Hz. The performance significantly increases from graph (e) and indicates that the mathematical model is responding most effectively to this frequency. The mathematical model of the oil/air mixed damper seems to be functioning optimally, as the damper's performance steadily improves with the frequencies. This suggests that the model accurately predicts the damper's behavior and effectively measures its performance. Consequently, this mathematical model serves as an efficient tool for forecasting the performance of the oil/air mixed damper.

The damper's ability to reduce vibrations or oscillatory motion is determined by its damping force. Graphs (g) and (h) show that the oil/air mixed damper has a damping ratio of approximately 40% at 10 Hz and 12 Hz compared to 2 Hz. This indicates that the damper is working efficiently, reducing vibrations at these frequencies. As the frequency increases, the damper's effectiveness in reducing vibrations is illustrated by a higher damping ratio.

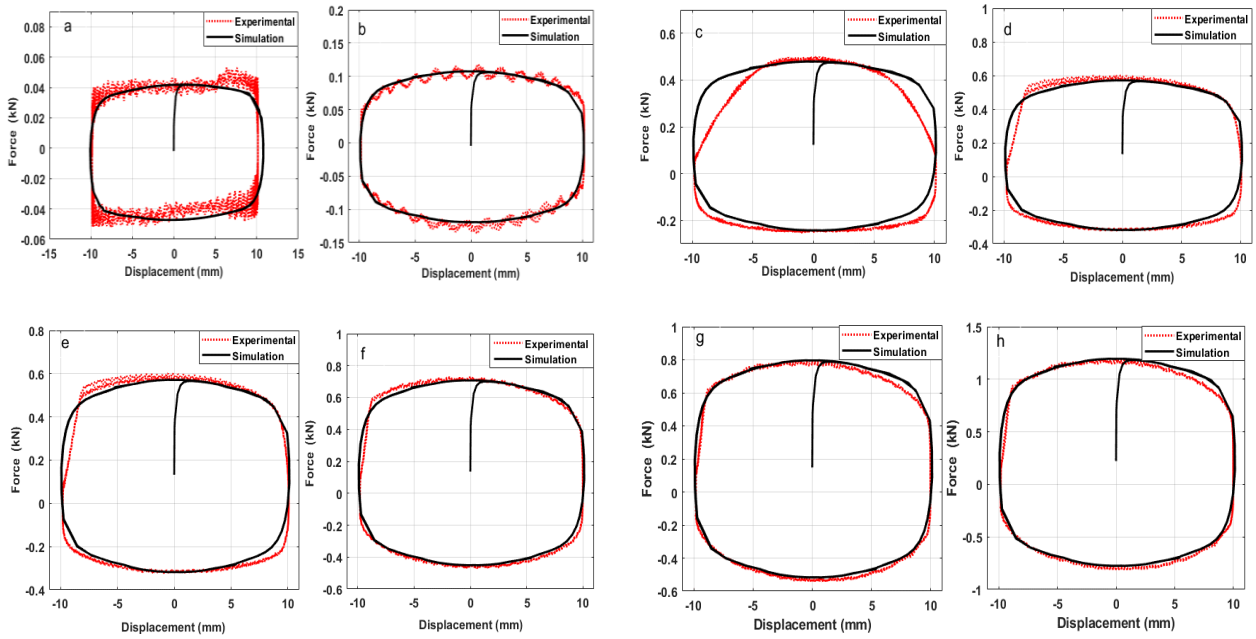

Figure 7. Comparison of the model and experimental data using force versus displacement based on an Amplitude of 10 mm at different frequencies: (a) 0.05 Hz; (b) 0.5 Hz; (c) 2 Hz; (d) 4 Hz; (e) 6 Hz; (f) 8 Hz; (g) 10 Hz; (h) 12 Hz

4. VEHICLE SUSPENSION MODEL

The two-degree-of-freedom (2-DOF) system used to illustrate the quarter vehicle suspension concept is depicted in Figure 8. It involves a sprung greater mass (m_b) denoting the body mass, un-sprung lower mass (m_w) denoting the wheel mass. The vertical motions of both m_b and m_w are qualified by the displacements X_b and X_w, respectively. Additionally, the excitement caused by a road disturbance is explained by X_r. The stiffness and damping properties of the suspension system are also denoted by K_s and C_s, and the tire spring stiffness is denoted by K_t. Tire damping is assumed to be neglected. Based on the vehicle ride model and Newton's second law, the equations of motion are provided by:

$$m_b\ddot{X}_b + C_s(\dot{X}_b - \dot{X}_w) + K_s(X_b - X_w) - U_f + u = 0 \tag{15}$$

$$m_w\ddot{X}_w - C_s(\dot{X}_b - \dot{X}_w) - K_s(X_b - X_w) + K_t(X_w - X_r) - u = 0 \tag{16}$$

For the proposed active suspension system, the active control force (u) depends on the relative displacement x_{relative} and relative velocity $\dot{x}_{\text{relative}}$ between sprung mass and un-sprung mass across it:

$$x_{\text{relative}} = X_b - X_w \quad \& \quad \dot{x}_{\text{relative}} = \dot{X}_b - \dot{X}_w \tag{17}$$

Two types of road excitations are selected and compared with the passive suspension system to assess the effectiveness of proposed alternative control strategies for the active suspension system. The transient response characteristics of a system can be revealed by utilizing the first excitation, often known as a road bump. This initial disturbance aids in comprehending the system's response to abrupt changes and offers valuable insights into its behavior. The first excitation can be described as follows:

$$X_r(t) = \begin{cases} a\left[1 - cos\left[\frac{2\pi U_o}{d}(t - 0.5)\right]\right], for\ \ 0.5 \le t \le 0.5 + \frac{d}{U_o} \\ 0, \qquad\qquad otherwise \end{cases} \tag{18}$$

where $d, U,$ and a are the bump's width, the speed of the vehicle, and the bump's half amplitude. The parameters' values are as follows: d =0.8 m, U_o =0.856 m/sec, and a =0.035 m, respectively. A random road profile, which is the second type of road excitation, is frequently used to evaluate the frequency response of road surfaces. This method involves subjecting vehicles or structural elements to unpredictable road conditions, simulating real-world scenarios. The road roughness disturbance is determined through a standardized process that involves various measurements and assessments. The following is a description of the random road disturbance:

$$\dot{X}_r(t) = -2\pi f_o X_r(t) + 2\pi\sqrt{G_O U_O}\omega(t) \tag{19}$$

where: the low cut-off frequency is f_o, the coefficient of road irregularities is G_O. When driving on a paved road, the vehicle's velocity is U_o=20 m/s and the Gauss white noise is $\omega(t)$.Also, the road displacement input is $X_r(t)$.

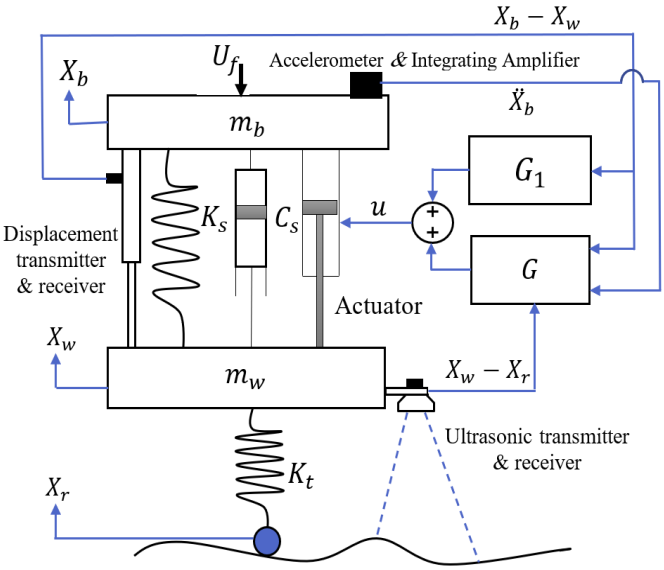

Figure 8. Active suspension system's vehicle ride model

In the state space form, the suggested active suspension system can be shown as follows:

$$\ddot{X} = A\,X + B\,u + D\,\omega(t) \tag{20}$$

$$A = \begin{bmatrix} 0 & 0 & 1 & 0 & 0 & 0 \\ 0 & 0 & 0 & 1 & 0 & 0 \\ \frac{-K_s}{m_b} & \frac{K_s}{m_b} & \frac{-C_s}{m_b} & \frac{C_s}{m_b} & 0 & 0 \\ \frac{K_s}{m_w} & \frac{-K_s+K_t}{m_w} & \frac{C_s}{m_w} & \frac{-C_s}{m_w} & 0 & \frac{K_t}{m_w} \\ 0 & 0 & 0 & 0 & \frac{-1}{m_b} & 0 \\ 0 & 0 & 0 & 0 & 0 & -2\pi f_o \end{bmatrix}, B = \begin{bmatrix} 0 \\ 0 \\ \frac{-1}{m_b} \\ \frac{1}{m_w} \\ 0 \\ 0 \end{bmatrix}, \text{and } D = \begin{bmatrix} 0 \\ 0 \\ 0 \\ \frac{K_t}{m_w} \\ 0 \\ 2\pi\sqrt{G_o U_o} \end{bmatrix}$$

where: the state variables are denoted by $X = [X_b\,, X_w\,, \dot{X}_b\,, \dot{X}_w\,, U_f,\ X_r\,]^T$, the control input matrix denotes by B, the active control force denotes by u, the disturbance input matrix denotes by D, and the road profile is described by X_r. u(N) is determined by the hybrid control method in this research, and U_f is the vehicle body's external force (N).

4.1 Hybrid Controller Design

The hybrid control system, which combines the PID controller with the LQR controller, is intended to estimate the ideal active control force in real-time. The PID controller is utilized to create a zero steady-state offset, and the LQR controller is used to enhance suspension performance criteria. Thereby, the active control suspension system reacts quickly under variable external loads. Ride comfort, road-holding ability, and suspension working space are the three measures that can be used to evaluate the main performance criteria in vehicle suspension design. The ride comfort of a vehicle is significantly influenced by the body acceleration it experiences. Body acceleration refers to the rate at which the vehicle's body moves or changes speed. It is a crucial factor in determining the overall comfort level of passengers during a ride. Minimizing excessive body acceleration through proposed suspension systems and optimized vehicle design helps to enhance the overall comfort for passengers. Minimizing tire load variation offers several benefits. Firstly, it enhances the vehicle's handling and responsiveness, allowing for more precise steering control. This is particularly important when navigating corners or making quick maneuvers. By minimizing the tire's deformation, the vehicle's stability is improved, reducing the risk of skidding or loss of control. The structural characteristics of a vehicle play a crucial role in determining the amount of suspension working space available. These structural features impose constraints and limitations on the suspension system, dictating its range of motion and maximum extension. The design of the vehicle,

including factors such as the wheelbase, chassis stiffness, and overall weight distribution, directly influences the available space for the suspension system to operate effectively. Thereby, the suspension performance can be improved by minimizing the suspension working space, reducing body acceleration, and optimizing dynamic tire load.

The LQR control problem is formulated to achieve better magnitudes of the main performance criteria based on the optimal active control force(u). The definition of the performance function J is as follows:

$$J = \lim_{T\to\infty} \frac{1}{2T}\, E \int_0^T [q_1\, \ddot{X}_b{}^2 + \, q_2\, (X_b - X_w)^2 + q_3\, (X_w - X_r)^2 + \, \rho u^2]\ \mathrm{d}t \tag{21}$$

The target performance evaluation function based on the performance index is provided in matrix form by

$$J = \lim_{T\to\infty} \frac{1}{2T}\, E \left[\int_0^T [X^T \quad u^T] \begin{bmatrix} Q & N \\ N^T & r_c \end{bmatrix} \begin{bmatrix} X \\ u \end{bmatrix} dt\right] \tag{22}$$

where:

$$Q = \frac{1}{m_b{}^2} \begin{bmatrix} s^2 + q_1 m_b{}^2 & 0 & -sc & sc & 0 & 0 \\ 0 & q_2 m_b{}^2 & 0 & 0 & 0 & 0 \\ -sc & 0 & c^2 & -c^2 & 0 & 0 \\ sc & 0 & -c^2 & c^2 & 0 & 0 \\ 0 & 0 & 0 & 0 & q_3 m_b{}^2 & 1 \\ 0 & 0 & 0 & 0 & 1 & 0 \end{bmatrix},$$

$$N = \frac{1}{m_b{}^2}[s \quad 0 \quad -c \quad c \quad 0 \quad 0]^T, \mathrm{r_c} = \frac{1}{\mathrm{m_b}{}^2} + \rho$$

where: $q_1, q_2,$ and q_3 are the body weights accelerating, suspension working space, road contact tire deflection, ρ is the weight on control force, Q is positive semi-definite, r_c is the positive definite, and N is the constant matrix. The control gain based on minimizing J for the system presented in Figure 8 as a full state feedback with respect to measurements, is given by

$$u = -R_c^{-1}[N^T + B^T P_c]\, X = \, -G\, X(t) \tag{23}$$

where: P_c is found through the solution of the Riccati equation given below:

$$A\, P_c + \, P_c A^T - P_c\, B\, r_c^{-1} P_c + \, Q = 0 \tag{24}$$

where: $A \in \Re^{6\times 6}$ and $B \in \Re^{6\times 1}$ are the system matrix and the control input matrix.

Therefore, the optimal active control force is formed as follows:

$$G = P_c\, B\, r_c^{-1} = K_1 X_b + K_2 X_w + K_3 \dot{X}_b + K_4 \dot{X}_w + K_5 X_5 \tag{25}$$

PID controller is also expressed based on its behavior and applicability as a leveling control. The equation describing the basic structure of this controller can be listed as follows:

$$G_1 = K_P (X_b - X_w)(t) + K_I \int_0^t (X_b - X_w)(t)\ dt \ + K_D \frac{d(X_b - X_w)}{dt} \tag{26}$$

where: K_P, K_I, and K_D are the proportional, integral, and the derivative gains

4.2 Optimal Active Control Force $(\boldsymbol{u = G + G_1})$

The PID and LQR optimal parameters can be determined using genetic algorithms (GA) within MATLAB Toolboxes. The primary objective is to achieve the best possible active control force. By employing a GA to optimize the PID-LQR algorithm's parameters, we can enhance the performance of the control system and achieve the desired control force. The GA mimics the process of natural evolution, starting with an initial population of potential solutions represented by a set of chromosomes, as illustrated in Figure 9. Each chromosome specifies the values of the PID-LQR algorithm's parameters, encoding a potential solution. Through crossover, mutation, and selection processes, new offspring are generated from these chromosomes. These offspring are then evaluated based on their fitness using the objective function. The next generation is composed of the fittest individuals, and this iterative process continues until the optimal solution is reached. The desired control performance is reflected in the objective function utilized in this optimization process. This function can be tailored to specific performance criteria, such as minimizing overshoot, settling time, or control error. By continuously assessing and enhancing the fitness of the population, the genetic algorithm converges towards the optimal set of parameters for the PID-LQR algorithm, ultimately leading to the optimal active control force.

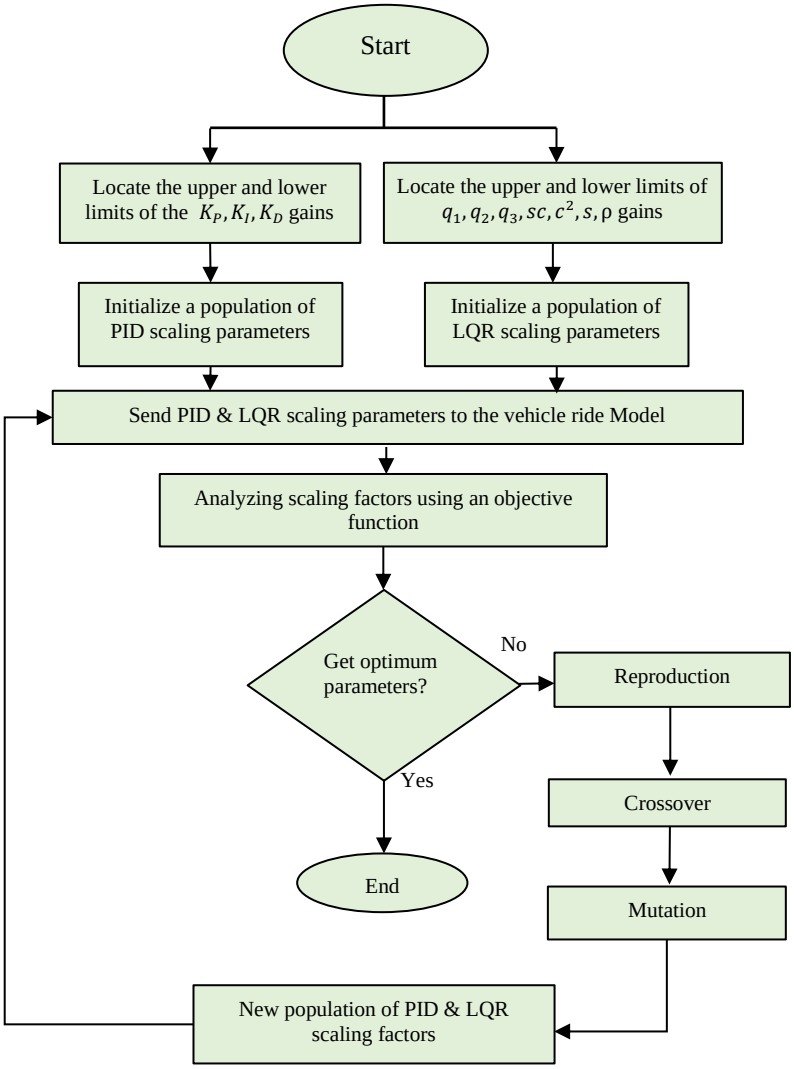

Figure 9. Flowchart provides a general overview of the main steps in a GA

5. RESULTS AND DISCUSSION

The SUVs' suspension systems served as the basis for the validated model used in the simulation. This indicates that the model, which underwent testing and validation, accurately reflects the behavior and functionality of the suspension system in real SUVs. The data collected from spring and damper testing offers valuable insights into the actual behavior of the suspension components. This data can help determine the stiffness and damping rates of the SUVs' suspension system, considering the interaction between the sprung and un-sprung masses. By integrating these actual values into the simulation, the model becomes more representative of the real-world system. This is crucial for studying and analyzing the suspension system's performance, as it enhances understanding of how the system will respond in different conditions and scenarios. The study utilized the following common set of baseline values:

Sprung mass, $m_b = 375.25$ kg
Un-sprung mass, $m_w = 37.81$ kg
Tire spring rate, $K_t = 230000$ N/m

These values are used as a starting point for the simulation and can be used to simulate an SUV's passive suspension system. By iteratively adjusting the spring constant and damping coefficient and analyzing the simulation results, the performance of the active suspension system can be enhanced for different road conditions. This modified design can provide improved ride comfort, better handling, and increased stability for SUVs. By incorporating passive elements, the reliance on active elements is reduced, leading to a lower power demand for the operation of the active elements. This is because the passive elements already provide a certain level of performance and safety, reducing the workload on the active elements. Consequently, the power consumption of the active elements can be minimized, resulting in improved energy efficiency and potentially extending the lifespan of the active components. The analysis of suspension performance in relation to vibration control is the main topic of this section. To gain a thorough understanding of the efficacy of various suspension systems, an analysis and evaluation of four cases will be conducted: (a) Passive suspension systems used for SUVs include real performances of both spring and damper tested by the MTS machine. The purpose of the suspension system is to absorb shocks and vibrations during driving to give a comfortable ride. However, passive suspension systems

cannot adjust to changing road conditions or driving styles. (b) The PID controller continuously monitors the vehicle's motion and calculates the appropriate adjustments needed to optimize the damping and stiffness of the suspension system. (c) Active suspension is used as a Linear Quadratic Regulator (LQR) control system to adjust the system in real time. In an active suspension system, the LQR controller considers the current state of the vehicle, such as its body acceleration, suspension deflection, and tire deflection, as well as the desired behavior of the suspension system. The controller then calculates the optimal control inputs, such as the damping and stiffness coefficients, that will minimize the cost function and achieve the desired behavior. (d) The hybrid controller modifies the suspension system in real time by combining the advantages of the PID and LQR controllers. Depending on the vehicle's operating conditions at the time, the hybrid controller can be configured to alternate between PID and LQR control. For instance, the controller may transition to linear speed regulation (LQR) if the vehicle surpasses a predetermined speed limit or if the road surface becomes excessively uneven.

5.1 Response of the Suspension System Under Bump Excitation

These values are used as a starting point for the simulation and can be used to simulate an SUV's passive suspension system. By iteratively adjusting the spring constant and damping coefficient and analyzing the simulation results, the performance of the active suspension system can be enhanced for different road conditions. This modified design can provide improved ride comfort, better handling, and increased stability for SUVs. By incorporating passive elements, the reliance on active elements is reduced, leading to lower power consumption. Figure 10(a)–(d) displays the suspension system's behavior and performance over a specified time history. An active suspension system generally offers more advanced capabilities to absorb shocks, maintain stability, and ensure passenger comfort compared to a passive suspension system. Therefore, it is essential to consider the design, implementation, and quality of the controller when comparing the performance and effectiveness of active suspension systems. The road surface irregularities or vertical movement that the suspension system must react to are depicted in Figure 10(a). In comparison to other systems, the hybrid controller-based active suspension system's ability to absorb road disturbances and maintain stability can be better developed by examining the vertical displacement of the suspension system, as shown in Figure 10(b). Figure 10(c) illustrates the acceleration response experienced by the vehicle's body because of the road input signal. It provides information about the level of vibration and movement transmitted to the vehicle's occupants. Active suspension systems produce lower values, which indicate a smoother and more comfortable ride, whereas passive suspension systems produce higher values, which indicate a more jarring and uncomfortable ride. The load variation experienced by the vehicle's tires because of the road input signal, known as dynamic tire load, is depicted in Figure 10(d). This Figure shows how the hybrid controller-based active suspension system distributes and regulates the forces applied to the tires to maximize traction and stability. Additionally, the LQR-PID controller design in the active suspension system can lessen tire load variations.

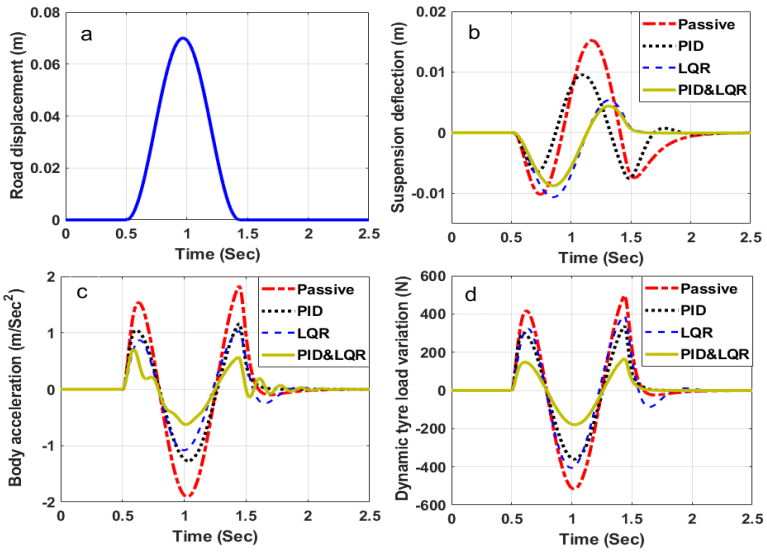

Figure 10. Time histories of the system's responses when excited by bumps in the road: (a) displacement of the road; (b) suspension deflection; (c) body acceleration; (d) dynamic tire load

5.2 State Reaction for Dynamic Suspension Systems with a Step Body Force of 1000 N

Figure 11(a)-(d) illustrates how different vehicle suspension designs respond to a 1000 N step force. Various suspension designs may demonstrate different levels of responsiveness and effectiveness in managing the applied force. The step force applied to the sprung upper mass is depicted in Figure 11(a), while Figures 11(b), 11(c), and 11(d) present the vehicle dynamic criteria. The results indicate that the LQR-PID controller-based active suspension system can achieve a zero steady-state offset, where the control system's output reaches and maintains error-free operation at the desired setpoint. This means the system can accurately follow the setpoint without any offset or steady-state error. Additionally, the LQR-PID controller can function resiliently in the face of external disturbances and changes in the vehicle's operating conditions, which is crucial for maintaining desired handling and ride characteristics across various driving scenarios.

Moreover, the LQR-PID controller seems to reduce oscillations caused by body acceleration more rapidly than the PID controller. This could be attributed to the integral terms in the LQR and PID controllers, allowing them to continuously adjust the control signal based on the accumulated error between the setpoint and the actual process variations. In contrast, the PID controller may not swiftly dampen system oscillations as it solely focuses on the suspension deflection error between the process variable and the setpoint.

The LQR controller is not very effective at rapidly reducing system offset despite performing well in many scenarios. This is due to its focus solely on the suspension deflection error. Other factors, such as delays and system dynamics, can also impact the speed at which oscillations are dampened. One contributing factor to this limitation is that the LQR controller heavily relies on the system's state variables in its feedback loop. These variables offer insights into the current system state, enabling the controller to adjust control inputs accordingly. However, delays within the system, like sensor response times or communication delays, can lead to discrepancies between the measured state variables and the actual system state. This discrepancy can hinder the LQR controller's ability to promptly react and minimize system offset.

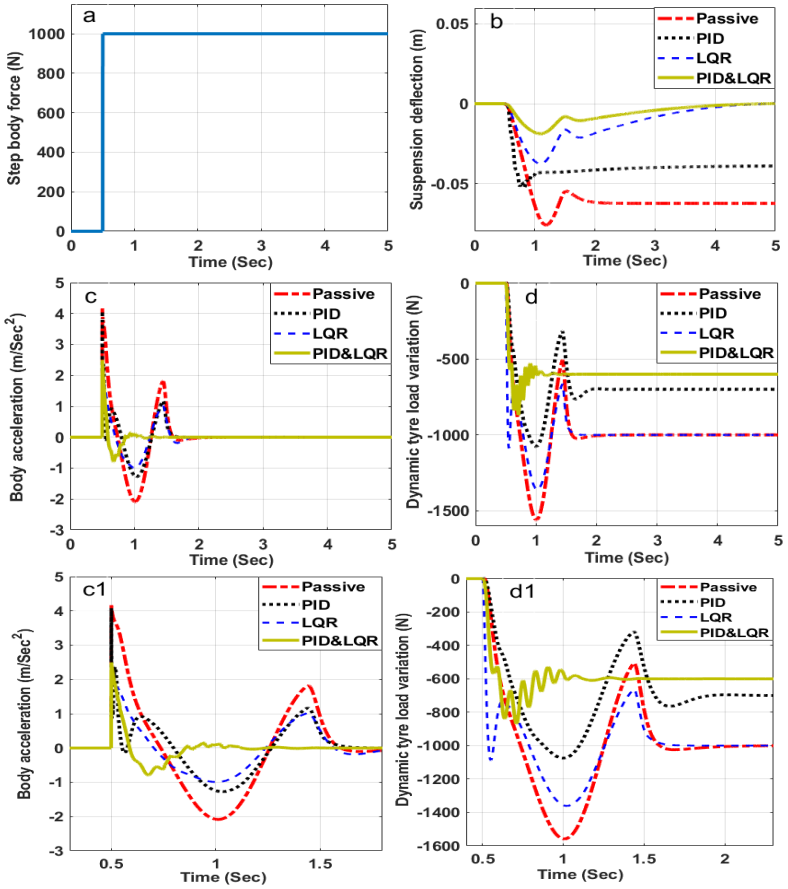

Figure 11. A vehicle's response to different controller designs: (a) step body force of 1000 N; (b) suspension deflection; (c) body acceleration (zoomed); (d) dynamic tire load variation (zoomed)

5.3 Control Force Generated Based on Road Bump Excitation

Figure 12(a)–(d) illustrates that in situations without and with step body force, the PID controller requires higher values of control force and power consumption compared to the LQR controller. This is because the PID controller operates by integrating three distinct control actions: derivative, integral, and proportional. The PID controller is effective in reducing a steady state offset due to its ability to adapt to changes in the active suspension system. However, the trade-off for this adaptability is increased control force and power consumption. On the contrary, the LQR controller presents a different approach. It focuses on minimizing a quadratic cost function to optimize the controller's performance. In contrast to the PID controller, the LQR controller necessitates lower values of control force and power consumption. This is achieved through the utilization of a state-feedback control law that considers the system's dynamics and desired performance criteria. To leverage the strengths of both controllers, the LQR-PID controller is introduced. The LQR-PID controller aims to find a middle ground between control force, power consumption, and performance. By merging the LQR and PID control methodologies, the LQR-PID controller can deliver superior control performance while maintaining lower levels of control force and power consumption compared to the PID controller alone.

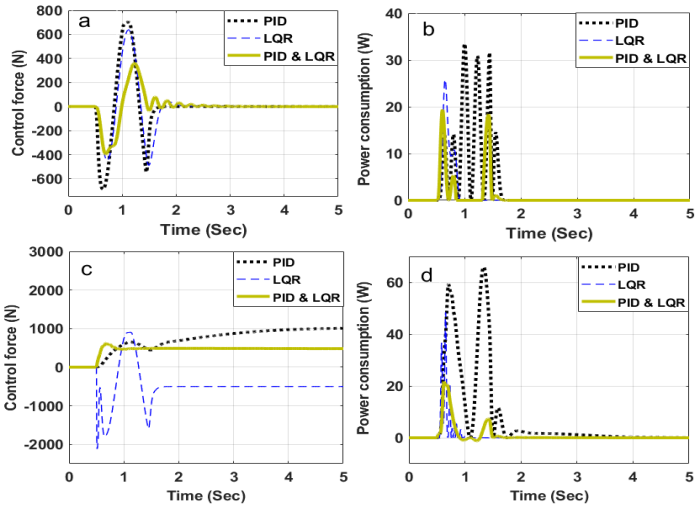

Figure 12. Control force and power consumption: (a)-(b) without step body force; (c)-(d) with step body force

5.4 Response of the Suspension System under Random Road Excitation

The vehicle's body must be shielded from road disturbances, and its body mass's resonance peak decreased to about 1 Hz in order to enhance ride comfort. The human body is known to be sensitive to this frequency, which has a significant effect on passenger comfort. When the body mass resonance peak is reduced or shifted away from this frequency, the perceived discomfort caused by vibrations is significantly minimized. In the pursuit of enhancing vehicle stability, it becomes crucial to maintain consistent contact between the tire and the road surface. This serves the purpose of minimizing the resonance peak that occurs around 10 Hz, as this frequency represents the resonance frequency of the wheel. Therefore, it is essential to prioritize measures that ensure the tire remains in constant contact with the road surface, thereby mitigating any potential negative effects of the resonance peak and promoting a smoother and safer driving experience. The results obtained for the excitation given by equation (19) are now presented in the frequency domain considering the previously mentioned considerations. This conversion makes it possible to thoroughly examine the excitation signal at various frequencies. The signal described as random road excitation is shown in Figure 13(a). The fast Fourier transform (FFT) modulus is a tool used to analyze the frequency domain characteristics of a signal. The FFT modulus can be used to analyze suspension responses and offer important information about how the suspension system behaves between 0 and 20 Hz. Figure 13(b)–(d) displays the frequency response of an active suspension system with the PID controller. The active system's frequency response curve is flatter and has a lower resonance peak than the passive suspension systems.

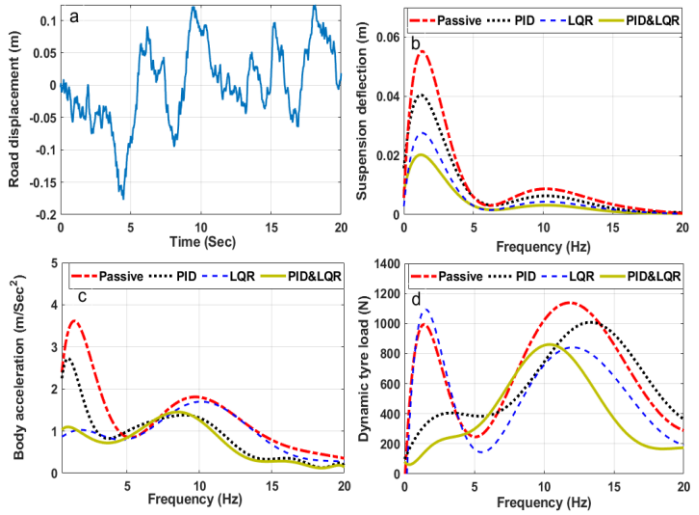

Figure 13. Chronologies of suspension system reactions when the road is randomly stimulated: (a) road displacement; (b) suspension deflection; (c) body acceleration; (d) dynamic tire load

This suggests that compared to the passive system, the active system is more capable of absorbing road disturbances and offering a smoother ride. When comparing the LQR controller to the active system, we can also observe that the latter has a more accurate and responsive frequency response. This implies that the LQR controller can adapt to changing road conditions more effectively, providing a more comfortable ride. Moreover, the increase in low-frequency stroke response indicates that the controlled suspension system offers a more compliant response to low-frequency road disturbances. This can be advantageous for absorbing larger, low-frequency road irregularities and enhancing overall ride comfort.

Graphs (b)–(d) illustrate how the LQR-PID controller strategy can effectively reduce resonance peaks in the vehicle's body and wheels. This control method is particularly adept at dissipating the energy generated by road excitation, thereby improving stability and comfort during the ride.

5.5 Control force generated based on random road excitation

Figure 14(a)–(b) shows a comparison of control force and power consumption among three different control strategies: PID, LQR, and PID-LQR, under random road excitation. The control force refers to the force applied by the controller to the system to maintain stability and minimize deviation from the desired response. Power consumption indicates the amount of energy consumed by the controller to ensure system stability. The FFT analysis for the control force reveals that in the low-frequency range of 0 to 3 Hz, the PID controller requires a higher control force compared to the LQR controller. This suggests that the PID controller needs more force to maintain stability and minimize deviation in this frequency range. Conversely, in the frequency range of 3 to 8 Hz, the LQR controller exhibits higher control force demand than the PID controller. This implies that the LQR controller needs more force in this frequency range to achieve stability and minimize deviation. The PID-LQR controller is designed to strike a balance between performance and stability, aiming to minimize errors effectively.

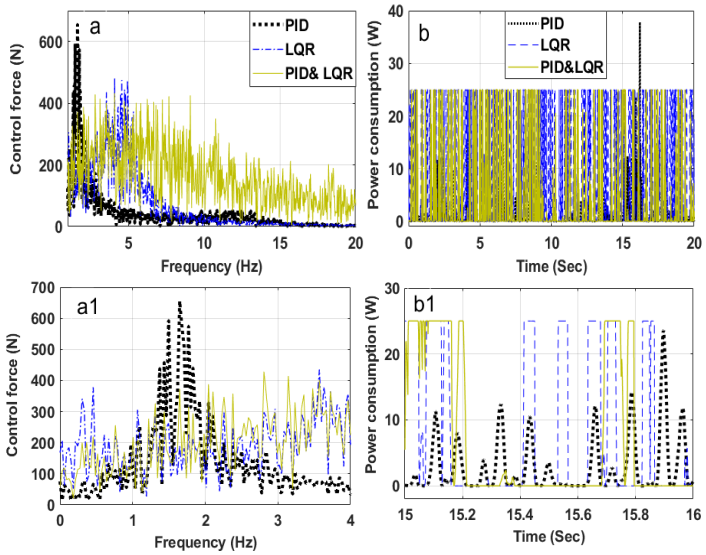

Figure 14(a)-(b). Controlling the force and power consumption required to overcome random road excitation

6. CONCLUSIONS

The performance evaluation of an active vehicle suspension system based on a PID-LQR controller designed in the time and frequency domains has revealed that the state variable feedback plus integral controller has great potential for providing excellent attitude control without compromising ride comfort. To assess the efficacy and reliability of this system, it was compared with passive and active suspension systems based on other controllers, including PID and LQR controllers. A mathematical model of a quarter-vehicle active suspension system was created based on SUV categorization, and both damping, and stiffness rates were assessed experimentally. This controller can offer a reliable and flexible method of managing the dynamics of a vehicle's suspension by combining the advantages of LQR based on state variable feedback and PID action. In greater depth, the PID-LQR controller is aimed at determining the desired damping force to minimize vibration levels while achieving zero steady-state suspension deflection. As demonstrated by the results, the recommended controller outperforms the passive suspension system in terms of ride comfort and driver stability.

ACKNOWLEDGEMENT

Experimental part of the work associated with the test rig measurements was conducted in the MTS Damper Test Machine in Tanks Department laboratory, Military Technical College (MTC), Cairo, Egypt.

REFERENCES

[1] J. D.-J. Lozoya-Santos, J. C. Tudon-Martinez, R. Morales-Menendez, O. Sename, A. Spaggiari and R. Ramírez-Mendoza, "A general modeling approach for shock absorbers: 2 Dof Mr Damper case study," *Frontiers in Materials*, vol. 7, p. 590328, 2021.

[2] S.W.R. Duym, "Simulation tools, modelling and identification, for an automotive shock absorber in the context of vehicle dynamics," *Vehicle System Dynamics*, vol. 33, pp. 261–285, 2000.

[3] M. Shams, R. Ebrahimi, A. Raoufi and B. J. Jafari, "CFD-Fea analysis of hydraulic shock absorber valve behavior," *International Journal of Automotive Technology*, vol. 5, pp. 615−622, 2007.

[4] N. Lavanya, P. Rao And M. Reddy, "Design and analysis of a suspension coil spring for automotive vehicle," international journal of engineering research and applications, vol. 9, pp. 151-157, 2014.

[5] L. Dai, M. Chi, H. Gao and J. Sun, "An investigation into the modeling methodology of the coil spring," *Hindawi Shock and Vibration*, vol. 2020, no. 1, p. 8814332, 2020.

[6] A. M. Wittek, D. Gąska, B. Łazarz and T. Matyja, "Coil springs in passenger cars – general theoretical principles and structural requirements," *The Archives of Automotive Engineering*, vol. 7, no. 2, pp. 141-159, 2016.

[7] H.B. Pawar, A.R. Patil and. S.B. Zope, "Design and analysis of a front suspension coil spring for three wheeler vehicle," *International Journal Of Innovations In Engineering Research and Technology*, vol. 3, pp. 1-10, 2016.

[8] N. Singh, "General review of mechanical springs used in automobiles suspension system," *International Journal Of Advanced Engineering Research and Studies*, vol. 115, p. 122, 2013.

[9] M. Rahman and S.B. Abdullah, "Numerical and experimental study on optimization of coil springs used in vehicles' suspension system," *Journal Of Engineering Advancements*, vol. 2, pp. 169-174, 2021.

[10] Y. Suda, S. Nakada and K. Nakano, "Hybrid suspension system with skyhook control and energy regeneration," *Vehicle System Dynamics*, vol. 28, pp. 619-634, 1998.

[11] B. Ebrahimi, H. Bolandhemmat, M. B. Khamesee and F. Golnaraghi, "A hybrid electromagnetic shock absorber for active vehicle suspension systems," *Vehicle System Dynamics*, vol. 49, pp. 311–332, 2011.

[12] K. Efatpenah, J. H. Beno and S. P. Nichols, "Energy requirements of a passive and an electromechanical active suspension system," *Vehicle System Dynamics*, vol. 34, pp. 437–458, 2000.

[13] H.H. Yuan Li, J. Z. Jiang, S. Burrow, S. Neild and A. Conn, "Enhancing the trade-off between ride comfort and active actuation requirements via an inerter-based passive-active-combined automotive suspension," *Vehicle System Dynamics*, vol. 62, no. 3, pp. 556-579, 2023.

[14] W. Huang, M. Ahmadian, A. Rahim and L. Steiginga, "Dynamics performance of long combination vehicles with active control systems," *Vehicle System Dynamics*, vol. 61, no. 7, pp.1831-1880, 2023.

[15] S. Liu, T. Zheng, D. Zhao, R. Hao and M. Yang, "Strongly perturbed sliding mode adaptive control of vehicle active suspension system considering actuator non-linearity," *Vehicle System Dynamics*, vol. 60, no. 2, pp. 597-616, 2022.

[16] V. Muniandy, P. Samin and H. Jamaluddin, "Application of a self-tuning fuzzy Pi–Pd controller in an active anti-roll bar system for a passenger car," *Vehicle System Dynamics*, vol. 53, no. 11, pp. 1641-1666, 2015.

[17] H. Gao, L. Jézéquel, E. Cabrol and . B. Vitry, "Chassis durability and comfort trade-off at early stage of project by virtual proving ground simulation," *Vehicle System Dynamics*, vol. 60, no. 6, pp. 2124-2144, 2022.

[18] G. Li, R. Wu, X. Deng, L. Shen and Y. Yao, "Suspension parameters matching of high-speed locomotive based on stability/comfort pareto optimization," *Vehicle System Dynamics*, vol. 60, no. 11, pp. 3848-3867, 2022.

[19] M. Čorić, J. Deur, L. Xu, H.E. Tseng and D. Hrovat, "Optimisation of active suspension control inputs for improved vehicle ride performance," *Vehicle System Dynamics*, vol. 54, no. 7, pp. 1004-1030, 2016.

[20] A.S. Gad and E.-D. Samir, "Effect of optimal fuzzy models for pneumatic magnetorheological suspension system on ride performance under different conditions," *SAE International Journal of Vehicle Dynamics, Stability, and NVH*, vol. 6, pp. 421-440, 2022.

[21] A. Shehata Gad, "Preview model predictive control controller for magnetorheological damper of semi-active suspension to improve both ride and handling," *SAE International Journal of Vehicle Dynamics, Stability, and NVH*, vol. 4, pp. 305-326, 2020.

[22] A. Shehata Gad, S. Darakhshan Jabeen, and W. Galal Ata, "Damping magnetorheological systems based on optimal neural networks preview control integrated with new hybrid fuzzy controller to improve ride comfort," *SAE Int. J. Veh. Dyn., Stab., and NVH*, vol. 7, no. 4, pp. 1-24, 2023.

[23] H. Han, B. Yim, N. Lee and Y. Kim, "Prediction of ride quality of a maglev vehicle using a full vehicle multibody dynamic model," *Vehicle System Dynamics*, vol. 47, no. 10, pp. 1271–1286, 2009.

[24] G. Geetharamani, K. Dhinakaran, J. Selvaraj and S.C. Ezhil Singh, "Sport-utility vehicle prediction based on machine learning approach," *Journal of Applied Research and Technology*, vol. 19, pp. 184-193, 2021.

[25] A. Khajepour and A. Soltani, "A coordinated control system for truck cabin suspension based on model predictive control," *International Journal Of Heavy Vehicle Systems*, vol. 29, p. 518–536, 2022.

[26] J. Liang, Y. Lu, D. Pi, G. Yin, W. Zhuang, F. Wang, J. Feng and C. Zhou, "A decentralized cooperative control framework for active steering and active suspension: Multi-agent approach," *IEEE Transactions on Transportation Electrification*, vol. 8, pp. 1414-1429, 2022.

[27] "Machine Learning for Autonomous Vehicle's Trajectory Prediction: A Comprehensive Survey, Challenges, And Future Research Directions," *Vehicular Communications*, vol. 46, p.100733, 2024.

[28] T.A. Nguyen, "A novel approach with a fuzzy sliding mode proportional integral control algorithm tuned by fuzzy method (FSMPIF)," *Scientific Reports*, vol. 13, no. 1, p.7327, 2023.

[29] D.N. Nguyen and T.A. Nguyen, "A novel hybrid control algorithm sliding mode-Pid for the active suspension system with state multivariable," *Complexity*, vol 2022, no. 1, p. 9527384, 2022.

[30] T.A. Nguyen, "Improving the stability of the passenger vehicle by using an active stabilizer bar controlled by the fuzzy method," *Hindawi Complexity*, vol 2021, no. 1, p. 6569298, 2021.

[31] Z.-J. Fu and X.-Y. Dong, "H∞ optimal control of vehicle active suspension systems in two time scales," *Journal For Control, Measurement, Electronics, Computing and Communications*, vol. 62, pp. 1-15, 2021.

[32] H. Yang, B.-G. Kim, J.-S. Oh and G.-W. Kim , "Simultaneous estimation of vehicle mass and unknown road roughness based on adaptive extended kalman filtering of suspension systems," *Electronics*, vol. 11, no. 16, pp. 1-15, 2022.

[33] Y. He, Y. Zhou, D. Wang, S. Liu and X. Wei, "Stabilization analysis of a class of nonlinear time delay systems with time-varying full-state constraints," *Journal for Control, Measurement, Electronics, Computing and Communications*, vol. 64, no. 3, pp. 496-507, 2023.

[34] S.-Y. Han, J.-F. Dong, J. Zhou and Y.-H. Chen, "Adaptive fuzzy Pid control strategy for vehicle active suspension based on road evaluation," *Electronics*, vol. 11, no. 6, p. 921, 2022.